# Reversible Bistable Switching in Nanoscale Thiol−Substituted Oligoaniline Molecular Junctions

**ARTICLE** *in* NANO LETTERS · JANUARY 2006

Impact Factor: 13.59 · DOI: 10.1021/nl051219k · Source: PubMed

NANO LETTERS

2005
Vol. 5, No. 12
2365−2372

# Reversible Bistable Switching in Nanoscale Thiol-Substituted Oligoaniline Molecular Junctions

**Lintao Cai,[†] Marco A. Cabassi,[†] Heayoung Yoon,[†] Orlando M. Cabarcos,[‡] Christine L. McGuiness,[‡] Austen K. Flatt,[§] David L. Allara,*[,‡] James M. Tour,*[,§] and Theresa S. Mayer*[,†]**

*Department of Electrical Engineering and Department of Chemistry and Materials Research Institute, The Pennsylvania State University, University Park, Pennsylvania 16802, and Department of Chemistry and Center for Nanoscale Science and Technology, Rice University, Houston, Texas 77005*

*Received June 27, 2005; Revised Manuscript Received October 20, 2005*

**ABSTRACT**

**Single molecular monolayers of oligoaniline dimers were integrated into sub-40-nm-diameter metal nanowires to form in-wire molecular junctions. These junctions exhibited reproducible room temperature bistable switching with zero-bias high- to low-current state conductance ratios of up to 50, switching threshold voltages of approximately ±1.5 V, and no measurable decay in the high-state current over 22 h. Such switching was not observed in similarly fabricated saturated dodecane (C12) or conjugated oligo(phenylene ethynylene) (OPE) molecular junctions. The low- and high-state current versus voltage was independent of temperature (10−300 K), suggesting that the dominant transport mechanism in these junctions is coherent tunneling. Inelastic electron tunneling spectra collected at 10 K show a change in the vibrational modes of the oligoaniline dimers when the junctions are switched from the low- to the high-current state. The results of these measurements suggest that the switching behavior is an inherent molecular feature that can be attributed to the oligoaniline dimer molecules that form the junction.**

Considerable activity is being directed toward developing defect tolerant logic architectures to circumvent challenges arising from aggressive device and circuit scaling. The ability to incorporate bistable molecular switches into ultrahigh-density reconfigurable fabrics provides a promising route to address this challenge.[1,2] To this end, significant advances are being made in developing an improved understanding of the mechanisms that determine the electrical transport properties in molecular junctions with metal and/or semiconductor contacts.[3−6] Junctions comprised of single molecules and self-assembled monolayers (SAMs) have been studied using a variety of test structures,[7−19] and technologically attractive nonlinear device properties such as negative differential resistance,[20−23] rectification,[24] and switching[25−29] have been demonstrated. In this letter, we report on the reversible bistable switching characteristics observed in nanoscale molecular junctions that incorporate SAMs of dithiol-terminated *N*-methyl-oligoaniline dimers[30] at the interface between two metal contacts.

Template-based nanofabrication methods were used to synthesize the in-wire metal−molecule−metal junctions studied here.[14,31,32] In this process, Au or Pd metal nanowire segments with an approximate length of 3 $\mu$m were electrodeposited in polycarbonate mesoporous membranes with a 35-nm nominal pore diameter. The conditions used to grow the bottom metal segments result in single-crystal nanowires of many metals, including Au and Pd. Our data suggest that this leads to the formation of highly organized, densely packed monolayers on the nanowire tips, thereby increasing the yields of junctions with reproducible electrical characteristics.[31] Following metal deposition, the membranes were rinsed thoroughly with deionized water and ethanol prior to transferring them into the solution for chemical assembly of active molecules shown in Figure 1A. A 0.25 mM solution was made up of the molecules dissolved in a mixed solvent of ethanol, methanol, and acetone, which is compatible for use with the polycarbonate membranes. As shown in Figure 1A, molecules of [4-({4-[(4-acetylsulfanyl-phenyl)-methyl-amino]-phenyl}-methyl-amino)-phenyl] having either thioacetate (**1a**) or free-thiol (**1b**) end groups were used in this study. Self-assembly conditions were optimized for **1a** and

* Corresponding authors. E-mail: dla3@psu.edu; tour@rice.edu; tsm2@psu.edu.

[†] Department of Electrical Engineering, The Pennsylvania State University.

[‡] Department of Chemistry and Materials Research Institute, The Pennsylvania State University.

[§] Department of Chemistry and Center for Nanoscale Science and Technology, Rice University.

10.1021/nl051219k CCC: $30.25 
**Published on Web 11/12/2005**

**(A)**

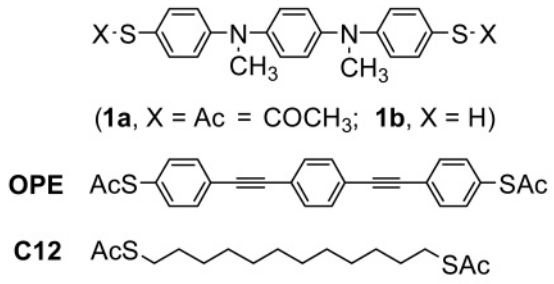


**(B)**

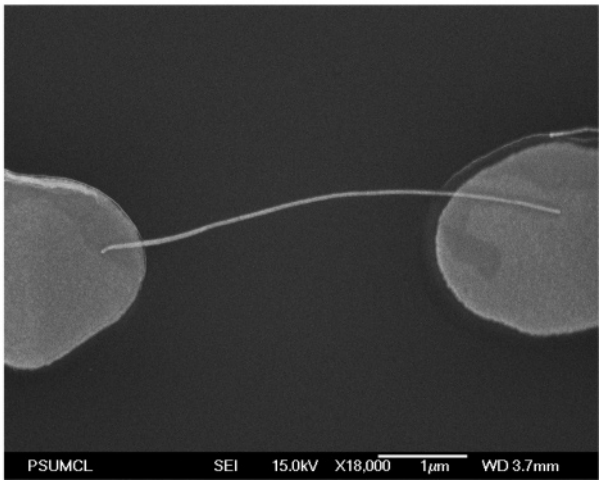


**Figure 1.** Molecules that were incorporated into the in-wire junctions studied here. (A) active molecules, (**1a**) the dithioacetate oligoaniline dimer, (**1b**) the dithiol oligoaniline dimer, and control dithioacetate molecules: oligo(phenylene ethynylene) (**OPE**) and dodecane (**C12**). (B) FE-SEM image of a 40-nm-diameter in-wire junction that is aligned between large area electrodes for measurement.

**1b** by first conducting experiments on planar evaporated Au or Pd substrates and then using these conditions to fabricate in-wire devices. All assembly was conducted in a glovebox with an inert atmosphere of $N_2$. For Au surfaces this involved (i) direct assembly from **1a** for 7 h, followed by deprotection of the topmost end group in dilute $NH_4OH$ for 5−10 min or (ii) direct assembly from **1b** for 5 h. For Pd surfaces this involved (i) deprotection of **1a** in dilute $NH_4OH$ followed by assembly for 2−5 h or (ii) direct assembly from **1b** for 5 h. For brevity, SAMs formed from **1a** and **1b** are designated SAM(**1a**) and SAM(**1b**), respectively. Single-wavelength (632.8 nm) ellipsometry of the SAMs prepared on planar surfaces yielded thicknesses consistent with those expected for single monolayer films. Moreover, studies of the same films using infrared reflection spectroscopy (IRS) confirmed the formation of well-organized monolayers from either **1a** or **1b**.[33] To aid in the interpretation of the IR spectra, geometry optimizations and frequency calculations of the neutral oligoaniline dimer were performed using density functional theory (DFT) at the 6-31G*//B3PW91 level of theory.

The in-wire junction synthesis was completed by forming a thin Pd seed metal layer that served as a top electrical contact, and then electrodepositing the second 3-$\mu$m-long Pd nanowire segments. The seed layer consists of a film of coalesced nanoparticles that was grown by electrochemical reduction of Pd metal ions adsorbed onto the free thiol end of the molecules from a solution of 3 mM $(NH_3)_4PdCl_2/H_2O$. This film serves as a protective layer that minimizes shorting of the molecular junction and as a seed layer to initiate growth of the top nanowire segment at a potential low enough to prevent desorption of the SAM (e.g., less than −0.4 V). This process allowed us to investigate the electrical properties of molecular junctions with asymmetric Au−SAM−Pd and symmetric Pd−SAM−Pd contacts.

Electrical testing was conducted on individual in-wire junctions after they were released from the template and aligned between pairs of large-area lithographically defined Au electrodes by AC electric-field-assisted assembly.[34] A field emission scanning electron microscope (FE-SEM) image of an aligned 40-nm-diameter nanowire junction is shown in Figure 1B. The electrical connection between the nanowire and contact pad is formed by physical contact during assembly, eliminating all high-temperature postprocessing steps that could impact the molecular junction properties. Control experiments made on solid Au and Pd nanowires show that the resistance associated with contact between the nanowire and electrodes is consistently less than 100 Ω, which is significantly lower than the resistance of the molecular junction. Moreover, the leakage current measured between two open contact pads is less than 200 fA at ±1 V. Thus, the current values reported here are those of the molecular junction.

Temperature-dependent current−voltage ($I-V(T)$) and switching measurements were performed in a variable temperature cryostat (10−300 K) under high vacuum conditions using an Agilent 4155C Semiconductor Parameter Analyzer. Inelastic electron tunneling (IET) spectra were obtained at 10 K using a standard AC modulation technique that employed a lock-in amplifier (Stanford Research Systems SR830) to collect the first or second harmonic signals, which are proportional to $dI/dV$ and $d^2I/dV^2$, respectively. An optimum balance between spectral resolution and signal-to-noise ratio (S/N) was achieved using an AC excitation voltage ($V_{rms}$) of ∼4 mV at 500 Hz modulation; lower values of $V_{rms}$ increased the spectral resolution but tended to degrade the signal quality. $d^2I/dV^2$ was obtained either directly from the average of 10−20 second harmonic measurement scans or by numerical differentiation from the average of 10−20 first harmonic measurement scans ($dI/dV$) and further smoothing using a five-point Savitzky-Golay routine. Comparison of IET spectra obtained from several junctions using both methods showed strong agreement in the peak positions and intensities.

Room-temperature $I-V$ characteristics of Au−SAM−Pd junctions fabricated using oligoaniline molecules (**1a**) are compared to those measured on control junctions comprised of either dodecane (C12) or oligo(phenylene ethynylene) (OPE) molecules in Figure 2A and 2B. A series of 10

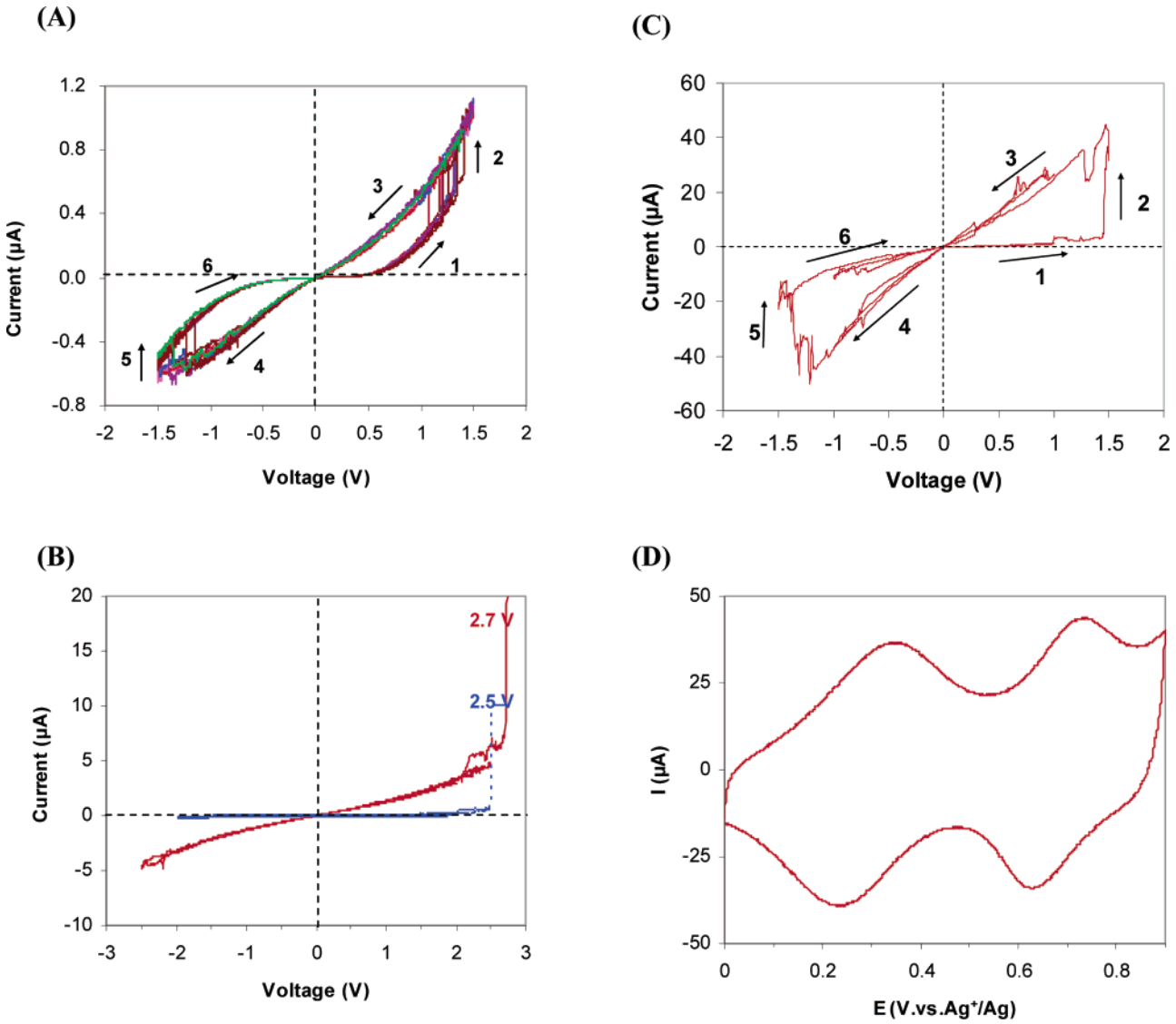


**Figure 2.** Typical room-temperature $I-V$ characteristics of (A) a Au−SAM(**1a**)−Pd in-wire molecular junction exhibiting a reversible switching behavior. Arrows show voltage sweep directions, (B) a Au−C12−Pd (dotted line) and Au−OPE−Pd (solid line) in-wire molecular junction that does not show hysteretic behavior, and (C) switching at a Pd−SAM(**1a**)−Pd in-wire molecular junction. (D) CV of SAM(**1a**) assembled onto a planar Au surface in 50 mM TBAP/$CH_2Cl_2$ measured at a scan rate of 50 mV/s.

successive $I-V$ sweeps collected by scanning the voltage in the direction indicated by the arrows labeled 1−6 demonstrate that the oliogoaniline junctions exhibit a stable and reversible hysteretic switching behavior. As the voltage bias is increased from 0 to +1.5 V, the current increases monotonically at low biases (1) until a sudden jump in current is observed at a positive threshold voltage ($V_T$) of approximately +1.5 V (2). The junction remains in the high current state as the voltage bias is increased to +1.5 V and lowered from +1.5 to 0 V (3). As shown in Figure 2A, the junction will remain in the low current state if the bias is not allowed to exceed this threshold voltage. Likewise, once the junction is switched to the high current state, it will stay in this state (3−4) until the junction is restored to its original, low current state (6) by sweeping the bias voltage to a negative threshold voltage of approximately −1.5 V (5). In these Au−Pd junctions, the ratio of the zero bias differential conductance between the two states is approximately 20.

More than 40 junctions of this type were characterized, including junctions from several different synthetic runs. Approximately 70% of these junctions exhibited a stable hysteretic behavior. The junction-to-junction variation in low-state current was within factor of 5 at 1 V, whereas that of the high-state current reached as high as a factor of 10 at 1 V. Such variations were observed previously for in-wire junctions[31] and can, at least in part, be attributed to differences in the junction areas that arise from variations in the membrane pore diameters and/or the fraction of molecules contacted by the top and bottom electrodes. The breakdown voltage of these Au−SAM(**1a**)−Pd junctions ranged from 2.4 to 2.7 V. This is consistent with the breakdown field strength[35] expected for a single monolayer of molecule **1a**, which provides evidence that the observed behavior is not due to the incorporation of a molecular multilayer within the junction.

Au−SAM(**1b**)−Pd and Pd−SAM(**1a**)−Pd junctions were also fabricated and exhibited similar switching characteristics. The Au−SAM(**1b**)−Pd junctions with free thiols had low- and high-state currents that fell within the bounds of variation measured for the Au−SAM(**1a**)−Pd junctions made from thioacetate endgroups. This suggests that any thioacetate-coupled molecules present in SAM(**1a**) can be neglected in these electrical measurements. The symmetric Pd−SAM-(**1a**)−Pd junctions (see Figure 2C) had higher currents and a larger zero bias high- to low-state conductance ratio of approximately 50. The higher currents can be attributed to the lower contact resistance associated with the thiol−Pd electrodes as compared to the thiol-Au contact, which was predicted theoretically[36] and observed previously in a number of molecular junction testbeds including the in-wire structure used here.[31,37] These data indicate that the bistable switching is not due to the use of Au metal contacts in the junction (i.e, Au−SAM−Pd vs Pd−SAM−Pd), which is more prone to form metal nanofilaments[38,39] in thin organic films than Pd.

In contrast, as illustrated in Figure 2B, control experiments performed on Au−C12−Pd and Au−OPE−Pd junctions synthesized using a similar process[31] display a very weak (less than 5%) variation in differential conductance as the voltage is swept between 0 and ±2 V. These junctions exhibit irreversible breakdown when at a bias of approximately 2.5 V for the C12 and 2.7 V for the OPE monolayers. The field strength[35] at which breakdown occurs ($\sim 1.5 \times 10^7$ V cm$^{-1}$) is also consistent with the formation of single monolayers within these junctions.

One notable difference between these junctions is the presence of a redox moiety in the *N*-methyl-oligoaniline dimer as compared to the C12 and OPE molecules. A cyclic voltammogram (CV) of SAM(**1a**) assembled on a planar Au surface that was collected in a neutral electrolyte solution of 50 mM tetrabutylammonium perchlorate (TBAP) is shown in Figure 2D. The CV contains two reversible, one-electron oxidation/reduction peaks at 0.35/0.23 V (vs $Ag^+/Ag$) and 0.74/0.62 V with a $\Delta E \approx 120$ mV, which is reproducible over 20+ cyclic scans and indicates that the SAM of **1a** is stable and robust. This behavior is consistent with a chemical change from the neutral, to the radical cationic, and then to the dicationic state of the molecule. These electrochemical properties are similar to the reversible transitions observed in the conducting polymer, poly(*N*-methylaniline),[40] as well as a *N*,*N*,*N*′,*N*′-tetramethyl-*p*-phenylenediamine(TMPD) derivative[41] known to undergo two reversible, one-electron oxidations. Such reversible chemical changes of the oligoaniline dimer will be concomitant with changes in its conformational and molecular electronic structure, which could give rise to the reversible switching properties observed in these in-wire junctions.

Variable temperature *I*−*V* measurements were conducted to more fully investigate the mechanisms responsible for transport in the low- and high-current state of the SAM(**1a**/**1b**) in-wire junctions. Symmetric Pd−Pd junctions were used in these experiments because they have the highest current and largest zero-bias resistance ratio of the junctions studied.[31] Full temperature sweeps (300−10 K) were first collected in the low-current state, followed by switching of the junction to the high-current state at 100 K, and a second full temperature sweep (10−300 K) in the high-current state. The resulting Arrhenius plots of ln(*I*) versus 1/*T* as a function of applied bias from 0.1 to 1.0 V (see Figure 3A and 3B) illustrate that the junction conductance is essentially temperature-independent over a wide range of test conditions and show that coherent tunneling (i.e., superexchange)[42] is the dominant transport mechanism for both states. Junctions that were swept beyond breakdown at room temperature displayed linear *I*−*V* behavior with no switching and typically displayed resistances as low as 1200 Ω, a value many times higher than the ∼100 Ω intrinsic resistance of a 40-nm-diameter Au nanowire. In addition, once damaged, the conductance cannot be restored to the original low current state by any applied voltage conditions and the junction current remains strongly temperature-dependent with a negative temperature coefficient. All of these properties are characteristic of a metallic junction,[43] which indicates that irreversible metal nanofilaments are formed at breakdown.

A previous study comparing thermally activated transport in junctions with individual isolated and densely packed monolayers comprised of the same $NO_2$-functionalized OPE (NOPE) molecules showed a suppression in the onset of thermally activated (i.e., hopping) transport in the SAM junctions (i.e., onset of thermally activated transport was observed near 125 K in isolated junctions, whereas the SAM junctions did not exhibit temperature dependence over the 10−300 K range).[32] It was suggested that the difference occurs because of changes in thermal and electrostatic effects that depend on the local molecular environment, which differs significantly for the two types of junctions. Although *I*−*V*(*T*) were not collected on individual oligoaniline molecules, the temperature-independent properties of the oligoaniline SAM junctions are consistent with these earlier findings. Here, it is also important to note that these junctions display two well-defined reversible conduction states. This indicates that the mechanism responsible for the observed switching properties affects the majority of the molecules participating in conduction at the onset of the threshold voltage. A similar two-state behavior was reported previously in junctions of bipyridyl-dinitro oligo(phenylene ethynylene)-dithiol (BPDN) and was attributed to a voltage-triggered switching behavior in the individual molecules that comprise the SAM junctions.[28] Further experiments are necessary to determine if the switching observed in these oligoaniline junctions results from changes in the individual molecules that make up the SAM or is due to a collective effect that is impacted by the neighboring molecules in the SAM.

The threshold voltage and storage time of the oligoaniline junctions were investigated at room and low temperatures. Figure 3C shows a single *I*−*V* sweep of the Pd−SAM(**1a**)−Pd junction measured at 100 K. The bias dependence at low voltages (i.e., less than 1.5 V) of the low- and high-state currents are the same as those measured at room temperature as expected from the *I*−*V*(*T*). However, the threshold voltage for switching increases as the junction operating temperature

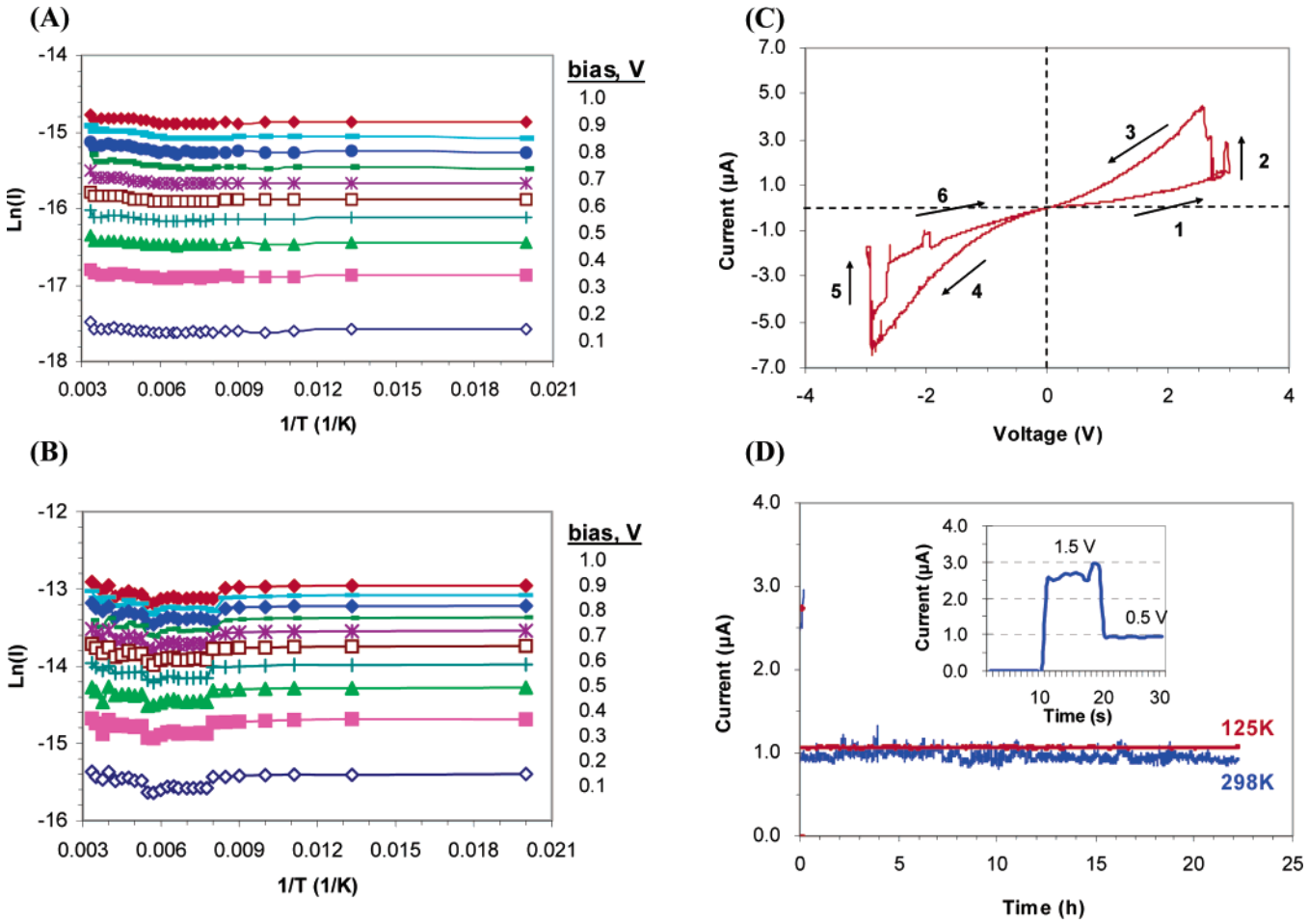


**Figure 3.** Arrhenius plot of a Pd−SAM(**1a**)−Pd in-wire molecular junction in the (A) low-current state and (B) high-current state. The junction current is shown as a function of temperature at fixed bias voltages ranging from 0.1 to 1.0 V in increments of 0.1 V as denoted in the figure. (C) Switching characteristics of the same junction measured at 100 K. (D) Transient response of the high-current state measured at 298 and 125 K. The inset shows the 0 to +1.5 V pulse that is applied for 10 s to switch the junction from the low- to the high-current state. The high-state current is detected at a constant bias of +0.5 V at 10-s intervals for a total duration of 22 h.

is reduced. In particular, the threshold voltage ($V_T$) is typically in the range of ±1.2 to ±1.5 V at 300 K, ± 2.7 to ±3.0 V at 100 K, and approximately ±3.5 V at 10 K. A plot of current as a function of time following the application of a voltage pulse that switched the junction from the low- to high-current state is shown in Figure 3D. These data were collected at a constant bias of +0.5 V for temperatures of 298 and 125 K. An inset of the first 30 s of the measurement gives the current measured before (0−10 s), during (10−20 s), and after the voltage pulse (+1.5 V) that was used to switch the junction from the low- to high-current state at 298 K. As expected from the $I-V$ sweep of this junction, the current increases rapidly at the rising edge of the voltage pulse, which corresponds to the transition between states. The high-state currents at 298 and 125 K are nearly equal and show no notable decay over the 22-h measurement period. The current measured at 125 K deviates less than ±0.5% from its median value, and the room-temperature scan shows larger ±5% fluctuation with time. The fluctuation is also observed in the Arrehenius plot (Figure 3B) for temperatures higher than 130 K. From a practical perspective, this change is negligible compared to the much larger difference in low- to high-state conductance measured for these junctions.

The long room temperature storage times observed in these oligoaniline junctions suggest that the switching behavior is not simply a result of a change in electronic state of the molecule, which would give rise to a shorter transient decay.[44,45] A more probable explanation for the data presented here is a chemical structure change involving a stable molecular conformation that can be reversed by applying a voltage exceeding $V_T$. The fluctuations in high-state current observed at temperatures above 130 K indicate that there are dynamic variations in the conductance through a small fraction of the molecules in the junction at higher temperatures. This effect must be explored more thoroughly in these and junctions comprised of other molecules to determine the source of the fluctuations.

Inelastic electron tunneling spectroscopy (IETS)[46,47] was used to measure the vibrational spectra of oligoaniline in-wire junctions in the low- and high-current states. These IET spectra can be used to assist one in developing an understanding of the possible mechanisms that are responsible for the observed bistable switching behavior of these junctions.

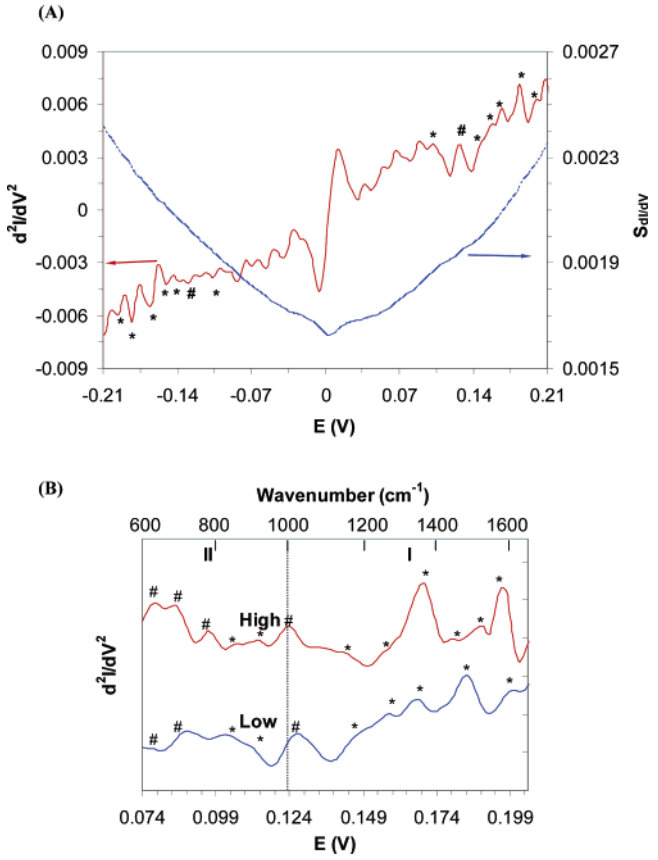


**Figure 4.** (A) IET spectrum showing positive and negative bias polarities for the low-current state of a Pd−SAM(**1a**)−Pd in-wire molecular junction determined by numerical differentiation of d*I*/d*V* using the procedure described in the text. The peaks identified by * (IR active) and # (Raman active) are those that are observed reproducibly in both bias polarities for a number of different oligoaniline junctions. (B) IET spectra of the low- and high-current state plotted for positive bias polarities; the assigned peaks have corresponding features in the negative bias polarity.

An IET spectrum of the low state of a Pd−SAM(**1a**)−Pd junction collected at 10 K for positive and negative bias polarities is shown in Figure 4A. The large zero-bias feature (ZBF)[48,49] contains low-frequency information unrelated to the bulk of the molecular bonding structure and is neglected in the analysis. Peak assignments were made using DFT calculations of the isolated oligoaniline dimer combined with IR and Raman spectra of mono- and dithiol oligoaniline SAMs on Au and bulk dithiol polycrystalline samples, respectively.[33] Peaks that were present in both the positive and negative bias scans are identified with star (IR active) and pound (Raman active) symbols. For analysis purposes, the vibrational spectrum of the oligoaniline dimer molecule is divided into two regions: 1660−1000 $cm^{-1}$ (Region I) containing the fundamental in-plane stretching modes, and 1000−600 $cm^{-1}$ (Region II) containing the out-of-plane, along with some low frequency in-plane, vibrational modes.[50,51]

The low current state Region I IETS peaks and their tentative assignments are the following: 198 mV [C═C stretching $\nu$(8a for Wilson notation)], 184 mV [C═C stretching $\nu$(8b)], 166 mV [C−N stretching with the inner ring C], 156 mV [C−N stretching with the outer ring], and 148 mV [C−H in-plane deformation]. An additional peak seen at 126 mV is consistent with a Raman active C−H deformation. Positive bias IET spectra for low- and high-current states of the same junction are shown in Figure 4B. Note that after the junction is switched to the high-current state, several of the Region I peaks are shifted to lower energies from those in the low-current state [e.g., $\nu$(8a), −2 mV; C−H in-plane deformation, −6 mV; C−H deformation, −2 mV]. Moreover, the 168 mV peak associated with the (aromatic C)−N stretch becomes broader and more intense, which suggests increases in the charge delocalization.[53] The peak 184 mV [$\nu$(8b)] feature disappears, replaced by two new peaks at 178 and 190 mV, which can be attributed to an antisymmetric C−N stretching mode and a C═N mode mixed with $\nu$(19a, C−C and CCH), respectively. Overall, these changes from the low- to high-current states demonstrate that corresponding changes occur in the electron delocalization around the N atoms and shift the associated bonding character.

The low current state Region II peaks and their tentative assignments are the following: 112 mV [$\delta$(C−H)], 102 mV [out-of-plane C−H bend], 88 mV [$\nu$(C−S) Raman active-1], and 78 mV [$\nu$(C−S) Raman active-2].[54] In switching to the high-current state, features assigned to these modes were observed at 114, 106, 86, and 78 mV and a new peak at 96 mV was assigned to a Raman active C−H mode. The occurrence of both positive and negative energy peak shifting is consistent with molecular structure changes, and the continued presence of the C−S stretching modes and metal-S modes (∼26 mV) shows that the molecule−electrode thiolate bonding remains intact upon switching.

Finally, we note that the most prominent peaks (e.g., $\nu$-(8a), $\nu$(8b) and the C−N stretching modes) are assigned to longitudinal vibrations parallel to the long molecular axis, which, in turn, is aligned along the nanowire axis and the charge flow across the biased junction. These modes thus could strongly couple with the tunneling charge carriers (i.e., a "through-bond" tunneling mechanism). In contrast, the relatively weak IETS peaks tend to involve vibrations with dipole motion perpendicular to the nanowire axis, for example, $\delta$(C−H) and out-of-plane C−H modes, which cannot couple with the charge carriers.

Several factors can be considered when trying to understand a molecular switching mechanism, including conformational changes with associated activation barriers between the structural states, electrostatic charge trapping at defects, metal nanofilaments, and metal-molecule contact interruptions. The combination of the temperature-independent $I-V$ behavior and molecular-based IETS data for the low- and high-current states eliminate explanations based on the operation of metal nanofilaments as the dominant mechanism.[18,38,39] Further, the essential invariance of the C−S modes in the IET spectra and the consistent intensities of the molecular peaks in the high- and low-current state spectra do not support metal−molecule contact breaking.[55,56] All of our data, however, is consistent with voltage-induced chemical structure change involving changes in molecular conformation with charge redistribution associated around the N centers. These changes could be somewhat similar in

character to electrochemically induced oxidation/reduction changes in the solution form of the molecule, that is, voltage-induced conversion of a neutral aniline dimer (low-current state) to an oxidized state (high-current state) with restoration under reverse bias. The intrinsic differences, however, between solid state and liquid−solid junctions preclude close comparisons.

In summary, we report the observation of a reversible and stable molecular switching in nanoscale in-wire junctions comprised of thiol-functionalized *N*-methyl-oligoaniline dimers with asymmetric Au−Pd and symmetric Pd−Pd contacts. These junctions show room-temperature zero-bias high- to low-state conductance ratios of up to 50, switching threshold voltages of approximately ±1.5 V, and high-state storage times much greater than 22 h. The low- and high-state currents versus voltage are independent of temperature over the range of 10−300 K, which suggests that the dominant transport mechanism in these junctions is coherent tunneling. The stability of the high-state current improves from ±5 to ±0.5% of its median value as the temperature was lowered to 130 K. IET spectra show a change in the vibrational modes of the molecular junction as it is switched from the low- to high-current state. Taken together, the data reported here suggest that reversible bistable switching properties observed in these junctions is an inherent molecular phenomenon, most likely arising from a concerted shift in charge delocalization and molecular conformation when the applied voltage across the molecular junction exceeds a critical threshold value.

**Acknowledgment.** This work was supported by the Defense Advance Research Projects Agency (DARPA) through the Office of Naval Research (ONR) under grant no. ONR-N00014-98-1-0846 (Penn State University) and grants of Rice University. Partial support was provided by NSF MRSEC, Center for Nanoscale Science, DMR-0213623. We also acknowledge insightful discussions with Dr. Hjalti Skulason and Professor Thomas Mallouk.

## References

(1) Goldstein, S. C.; Schmit, H.; Budiu, M.; Cadambi, S.; Moe, M.; Taylor, R. R. *Computer* **2000**, *33*, 70.
(2) Stan, M. R.; Franzon, P. D.; Goldstein, S. C.; Lach, J. C.; Ziegler, M. M. *Proc. IEEE* **2003**, *91*, 1940.
(3) Joachim, C.; Gimzewski, J. K.; Aviram, A. *Nature* **2000**, *408*, 541.
(4) Nitzan, A.; Ratner, M. A. *Science* **2003**, *300*, 1384.
(5) Rakshit, T.; Liang, G. C.; Ghosh, A. W.; Datta, S. *Nano Lett.* **2004**, *4*, 1803.
(6) Chen, Y. C.; Zwolak, M.; Di Ventra, M. *Nano Lett.* **2005**, *5*, 621.
(7) Andres, R. P.; Bein, T.; Dorogi, M.; Feng, S.; Henderson, J. I.; Kubiak, C. P.; Mahoney, W.; Osifchin, R. G.; Reifenberger, R. *Science* **1996**, *272*, 1323.
(8) Bumm, L. A.; Arnold, J. J.; Cygan, M. T.; Dunbar, T. D.; Burgin, T. P.; Jones, L.; Allara, D. L.; Tour, J. M.; Weiss, P. S. *Science* **1996**, *271*, 1705.
(9) Reed, M. A.; Zhou, C.; Muller, C. J.; Burgin, T. P.; Tour, J. M. *Science* **1997**, *278*, 252.
(10) Zhou, C.; Deshpande, M. R.; Reed, M. A.; Jones, L.; Tour, J. M. *Appl. Phys. Lett.* **1997**, *71*, 611.
(11) Cui, X. D.; Primak, A.; Zarate, X.; Tomfohr, J.; Sankey, O. F.; Moore, A. L.; Moore, T. A.; Gust, D.; Harris, G.; Lindsay, S. M. *Science* **2001**, *294*, 571.
(12) Holmlin, R. E.; Haag, R.; Chabinyc, M. L.; Ismagilov, R. F.; Cohen, A. E.; Terfort, A.; Rampi, M. A.; Whitesides, G. M. *J. Am. Chem. Soc.* **2001**, *123*, 5075.
(13) Kushmerick, J. G.; Holt, D. B.; Pollack, S. K.; Ratner, M. A.; Yang, J. C.; Schull, T. L.; Naciri, J.; Moore, M. H.; Shashidhar, R. *J. Am. Chem. Soc.* **2002**, *124*, 10654.
(14) Mbindyo, J. K. N.; Mallouk, T. E.; Mattzela, J. B.; Kratochvilova, I.; Razavi, B.; Jackson, T. N.; Mayer, T. S. *J. Am. Chem. Soc.* **2002**, *124*, 4020.
(15) Reichert, J.; Ochs, R.; Beckmann, D.; Weber, H. B.; Mayor, M.; von Lohneysen, H. *Phys. Rev. Lett.* **2002**, *88*, 176804.
(16) Wold, D. J.; Haag, R.; Rampi, M. A.; Frisbie, C. D. *J. Phys. Chem. B* **2002**, *106*, 2813.
(17) Loo, Y. L.; Lang, D. V.; Rogers, J. A.; Hsu, J. W. P. *Nano Lett.* **2003**, *3*, 913.
(18) Tour, J. M.; Cheng, L.; Nackashi, D. P.; Yao, Y. X.; Flatt, A. K.; St Angelo, S. K.; Mallouk, T. E.; Franzon, P. D. *J. Am. Chem. Soc.* **2003**, *125*, 13279.
(19) Selzer, Y.; Cabassi, M. A.; Mayer, T. S.; Allara, D. L. *J. Am. Chem. Soc.* **2004**, *126*, 4052.
(20) Chen, J.; Reed, M. A.; Rawlett, A. M.; Tour, J. M. *Science* **1999**, *286*, 1550.
(21) Le, J. D.; He, Y.; Hoye, T. R.; Mead, C. C.; Kiehl, R. A. *Appl. Phys. Lett.* **2003**, *83*, 5518.
(22) Guisinger, N. P.; Basu, R.; Greene, M. E.; Baluch, A. S.; Hersam, M. C. *Nanotechnology* **2004**, *15*, S452.
(23) Salomon, A.; Arad-Yellin, R.; Shanzer, A.; Karton, A.; Cahen, D. *J. Am. Chem. Soc.* **2004**, *126*, 11648.
(24) Metzger, R. M. *Synth. Met.* **2001**, *124*, 107.
(25) Collier, C. P.; Mattersteig, G.; Wong, E. W.; Luo, Y.; Beverly, K.; Sampaio, J.; Raymo, F. M.; Stoddart, J. F.; Heath, J. R. *Science* **2000**, *289*, 1172.
(26) Gittins, D. I.; Bethell, D.; Schiffrin, D. J.; Nichols, R. J. *Nature* **2000**, *408*, 67.
(27) Donhauser, Z. J.; Mantooth, B. A.; Kelly, K. F.; Bumm, L. A.; Monnell, J. D.; Stapleton, J. J.; Price, D. W.; Rawlett, A. M.; Allara, D. L.; Tour, J. M.; Weiss, P. S. *Science* **2001**, *292*, 2303.
(28) Blum, A. S.; Kushmerick, J. G.; Long, D. P.; Patterson, C. H.; Yang, J. C.; Henderson, J. C.; Yao, Y. X.; Tour, J. M.; Shashidhar, R.; Ratna, B. R. *Nat. Mater.* **2005**, *4*, 167.
(29) Chen, F.; He, J.; Nuckolls, C.; Roberts, T.; Klare, J. E.; Lindsay, S. *Nano Lett.* **2005**, *5*, 503.
(30) Flatt, A. K.; Tour, J. M. *Tetrahedron Lett.* **2003**, *44*, 6699.
(31) Cai, L. T.; Skulason, H.; Kushmerick, J. G.; Pollack, S. K.; Naciri, J.; Shashidhar, R.; Allara, D. L.; Mallouk, T. E.; Mayer, T. S. *J. Phys. Chem. B* **2004**, *108*, 2827.
(32) Selzer, Y.; Cai, L. T.; Cabassi, M. A.; Yao, Y. X.; Tour, J. M.; Mayer, T. S.; Allara, D. L. *Nano Lett.* **2005**, *5*, 61.
(33) The major IR peaks for the SAM(**1b**) on planar evaporated gold substrates were observed at: 1706, 1512, 1489, 1338, 1258, 1189, 1127, 1136, 1075, 929, and 820 $cm^{-1}$. The major Raman peaks in the bulk polycrystalline state of (**1b**) were observed at: 1706, 1610, 1587, 1430, 1361, 1258, 1188, 1103, 1069, 1001, 769, and 621 $cm^{-1}$. The electro-oxidation of SAM(**1a**) prepared on planar evaporated Au substrates was carried out at +0.75 V for 5 min at a neutral electrolyte. The sample was then rinsed and blown dry with $N_2$. The major IR peaks were observed at: 1711, 1622, 1576, 1508, 1486, 1420, 1354, 1331, 1260, 1187, 1125, 1093, 1069, 928, and 822 $cm^{-1}$.
(34) Smith, P. A.; Nordquist, C. D.; Jackson, T. N.; Mayer, T. S.; Martin, B. R.; Mbindyo, J.; Mallouk, T. E. *Appl. Phys. Lett.* **2000**, *77*, 1399.
(35) Wold, D. J.; Frisbie, C. D. *J. Am. Chem. Soc.* **2001**, *123*, 5549.
(36) Seminario, J. M.; De la Cruz, C. E.; Derosa, P. A. *J. Am. Chem. Soc.* **2001**, *123*, 5616.
(37) Chen, J.; Calvet, L. C.; Reed, M. A.; Carr, D. W.; Grubisha, D. S.; Bennett, D. W. *Chem. Phys. Lett.* **1999**, *313*, 741.
(38) Lau, C. N.; Stewart, D. R.; Williams, R. S.; Bockrath, M. *Nano Lett.* **2004**, *4*, 569.
(39) Stewart, D. R.; Ohlberg, D. A. A.; Beck, P. A.; Chen, Y.; Williams, R. S.; Jeppesen, J. O.; Nielsen, K. A.; Stoddart, J. F. *Nano Lett.* **2004**, *4*, 133.
(40) Lindfors, T.; Ivaska, A. *J. Electroanal. Chem.* **2002**, *535*, 65.
(41) Evans, R. G.; Klymenko, O. V.; Hardacre, C.; Seddon, K. R.; Compton, R. G. *J. Electroanal. Chem.* **2003**, *556*, 179.
(42) Segal, D.; Nitzan, A.; Davis, W. B.; Wasielewski, M. R.; Ratner, M. A. *J. Phys. Chem. B* **2000**, *104*, 3817.

(43) Kittel, C. *Introduction to Solid State Physics*, 7th ed; John Wiley & Sons: New York, 1996.
(44) Reed, M. A.; Chen, J.; Rawlett, A. M.; Price, D. W.; Tour, J. M. *Appl. Phys. Lett.* **2001**, *78*, 3735.
(45) Li, C.; Zhang, D. H.; Liu, X. L.; Han, S.; Tang, T.; Zhou, C. W.; Fan, W.; Koehne, J.; Han, J.; Meyyappan, M.; Rawlett, A. M.; Price, D. W.; Tour, J. M. *Appl. Phys. Lett.* **2003**, *82*, 645.
(46) Kushmerick, J. G.; Lazorcik, J.; Patterson, C. H.; Shashidhar, R.; Seferos, D. S.; Bazan, G. C. *Nano Lett.* **2004**, *4*, 639.
(47) Wang, W. Y.; Lee, T.; Kretzschmar, I.; Reed, M. A. *Nano Lett.* **2004**, *4*, 643.
(48) Gregory, S. *Phys. Rev. B* **1991**, *44*, 12868.
(49) Weber, H. B.; Haussler, R.; von Lohneysen, H.; Kroha, J. *Phys. Rev. B* **2001**, *6316*, 165426.
(50) Shacklette, L. W.; Wolf, J. F.; Gould, S.; Baughman, R. H. *J. Chem. Phys.* **1988**, *88*, 3955.
(51) Boyer, M. I.; Quillard, S.; Louarn, G.; Froyer, G.; Lefrant, S. *J. Phys. Chem. B* **2000**, *104*, 8952.
(52) DFT calculations at the 6-31G*//B3PW91 level of theory showed four different optimized geometries with energies ranging over a 0.4 kJ/mol spread. This result suggests that the potential energy surface of the isolated dimer is relatively flat, leading to a large number of accessible conformations. The frequency calculations also provided a good match to the spacings in the observed IR spectra of SAM (**1b**) on planar Au and Pd. Full details of these calculations and characterization of the monolayers will be reported elsewhere: McGuiness, C. L.; Cabarcos, O. M., Flatt, A. K., Cai, L. T., Tour, J. M., Mayer, T. S., Allara, D. L., manuscript in preparation.
(53) Grossmann, B.; Heinze, J.; Moll, T.; Palivan, C.; Ivan, S.; Gescheidt, G. *J. Phys. Chem. B* **2004**, *108*, 4669.
(54) Bryant, M. A.; Pemberton, J. E. *J. Am. Chem. Soc.* **1991**, *113*, 8284.
(55) Ramachandran, G. K.; Hopson, T. J.; Rawlett, A. M.; Nagahara, L. A.; Primak, A.; Lindsay, S. M. *Science* **2003**, *300*, 1413.
(56) Lewis, P. A.; Inman, C. E.; Yao, Y. X.; Tour, J. M.; Hutchison, J. E.; Weiss, P. S. *J. Am. Chem. Soc.* **2004**, *126*, 12214.

NL051219K